Tellus (2000), 52A, 365–379
Printed in UK. All rights reserved

TELLUS
ISSN 0280–6495

The impact of flow regimes on asymmetry of orographic drag at moderate and low Rossby numbers

By HARALDUR ÓLAFSSON*, *University of Iceland, Icelandic Meteorological Office and Institute for Meteorological Research, Bústadavegi 9, IS 150 Reykjavík, Iceland*

(Manuscript received 21 November 1997; in final form 3 November 1999)

ABSTRACT

The change of flow regimes from "flow over" (non-blocked flow) to "flow around" (blocked flow) is generally identified by flow stagnation upstream of the mountain and increased deflection of flow around the edges of the mountain. Numerical calculations of simple flow past a smooth mountain ridge presented here reveal another fundamental property of this change of flow regimes. In the presence of the Coriolis force, the drag exerts a cyclonic couple on non-blocked flows, but an anticyclonic couple on blocked flows. The delaying effect of the Coriolis force on the transition to the blocked flow regime is confirmed and the strength of the couple in blocked flows is also found to increase when the Rossby number U/fL decreases. A change in the flow regime from blocked to non-blocked flow when the Rossby number decreases gives a new high-drag regime at high non-dimensional mountain height (Nh/U) and increases substantially the temporal fluctuations of the drag. The sensitivity of the couple to the Rossby number is confirmed in realistic simulations of blocked flow from PYREX. Data from Iceland defines two regimes: at low Rossby number and high Nh/U, the drag on the right hand side is favoured, while at high Rossby numbers and low Nh/U the drag on the left side is larger.

1. Introduction

The decelerating effect of mountains on atmospheric flows has been investigated by numerous authors, ranging from the pioneering analytical models of 2D linear mountain waves by Queney (1948) and Eliassen and Palm (1960) to studies in three dimensions and of nonlinear vertically structured flow (see reviews by Smith, 1989 and Durran, 1990). Since orographic perturbations are believed to be a major sink of atmospheric momentum they have also gained the attention of numerical modelers in their need to account for the impact of non-resolved topography on the large scale flow (Lott and Miller, 1997; Broad, 1996; Beau and Bougeult, 1998). Orographic drag in blocked flow has also recently been modeled by Shutts (1998).

* e-mail: haraldur@vedur.is

In some of the preceeding literature, orographic drag is divided into form drag, wave drag and hydrostatic drag (Bessemoulin et al., 1993). The form drag is related to frictional forces, wave drag to vertically propagating gravity waves and the hydrostatic drag to accumulation of low level dense air above the upstream slopes of the mountain and descent of warm air in the lee. Thus, the term "hydrostatic drag" does not describe the total drag obtained by a hydrostatic model of frictionless flow or by integrating the hydrostatic equation up through the atmosphere on each side of the mountain. To avoid confusion we shall therefore not employ this term, but instead refer to descent of warm air in the lee or accumulation of cold air above the upstream slope or simply low level temperature anomalies. Unfortunately, the aforementioned low level temperature anomalies and the wave drag do not refer to separate terms in the momentum budget equations, and remain therefore

of a qualitative nature. However, we find such a classification useful, since in linear frictionless flow, the total drag is given by the wave drag, while in nonlinear blocked flow, the low level temperature anomalies are of significant importance.

For very small Rossby numbers ($\mathrm{Ro} = U/fL$, where U is the upstream wind speed, f is the Coriolis parameter and L is the alongstream mountain half-width), the orographic perturbations are dominated by lateral deflection and the gravity wave drag approaches zero. For increasing Rossby number, the mountain waves become more active and the maximum wave drag is obtained for infinite Rossby number. Analytic expressions of the restraining effect of the Coriolis force on the drag can be found in Gill (1982) and Smith (1979b).

Ólafsson and Bougeault (1997, hereafter ÓB97) have investigated the effect of rotation on orographic drag by simulating idealized flow with no Coriolis force and with $\mathrm{Ro} = 2.5$, which is a typical value for the Pyrenees. They found the Coriolis force to decrease the drag in the high drag regime of large amplitude breaking waves ($Nh/U \sim 1$, where N is the Brunt-Väisälä frequency, h is the mountain height and U is the upstream wind speed), but in the blocked regime at higher values of the upstream Nh/U, the rotation has the opposite effect: it increases the orographic drag and brings it closer to its linear value for this specific value of the Rossby number. That the Coriolis force increases the drag was found to be associated with increased accumulation of dense air above the upstream slopes, an effect that outweighs the well known reduction of wave drag predicted by linear theory. ÓB97 showed the drag for a case of blocked flow ($Nh/U = 2.7$) with the Coriolis force present to be slightly greater over the right flank than over the left flank of the mountain. This asymmetry was enhanced by surface friction.

In this paper, we continue to explore the orographic drag of an elongated mountain with Coriolis force. The study concentrates particularly on how the drag asymmetry, hereafter called a "couple", is affected by the regime of the flow and the Rossby number. A series of long numerical experiments with $\mathrm{Ro} = 0.5$ has been carried out and studied in connection with new aspects of some previous simulations with moderate and high values of the Rossby number. The drag for $\mathrm{Ro} = 0.5$ is compared to the results of ÓB97. The temporal evolution of the drag and the couple are studied, especially in connection to the Rossby number and flow regime. The effect of blocking and Rossby number on the transversal drag or "lift" force is also calculated and discussed. To illustrate the relevance of the Rossby number sensitivity of the couple within the blocked flow regime, we run a case of real flow from the PYREX field experiment. Finally, the impact of flow regimes on the couple is used to interpret real pressure data from Iceland. The paper discusses the importance of these findings for studies and parameterisation of orographic effects in the atmosphere.

In Section 2, there is a short description of the numerical model and the simulations that have been carried out. Section 3 describes the drag force as simulated in the experiments in the idealized flow. In Section 4, the temporal fluctuations and drag asymmetry (couple) are discussed. The real flows are presented in Section 5 and the paper concludes with a summary and a general discussion in Section 6.

2. The model and the numerical simulations

The calculations performed have been carried out with the PERIDOT hydrostatic numerical model developed by the French weather service (Imbard et al., 1986; Bougeault et al., 1991). PERIDOT has served for operational forecasting, as well as for numerous research projects in recent years. The experiments presented here have all been run with a 10 km horizontal resolution and with 40σ vertical levels ($\sigma = P/P_s$, where P is the pressure and P_s is the surface pressure). Above 12.6 km (two vertical wavelengths) there is a Rayleigh damping layer similar to that of Klemp and Lilly (1978). There is free slip at the lower boundaries. The mountain in the experiments with idealized flows is bell-shaped and given by the equation:

$$h(x, y) = \frac{h_{\max}}{[1 + (x/L_x)^2 + (y/L_y)^2]^{1.5}}, \qquad (1)$$

where $h_{\max}$ is the mountain height (hereafter h) and L_x and L_y are the mountain half-width and half-length. The aspect ratio $R = L_y/L_x$ is set to 5.

The initial conditions are the same everywhere in the simulation domain, but the values of N, h, U, and f differ from one simulation to another.

Table 1 summarizes the values of each of these parameters in all the simulations of flow past the bell-shaped mountain. The name of each simulation contains the value of the non-dimensional mountain height Nh/U and the Rossby number. EX27R25 is thus an experiment with $Nh/U = 2.7$ and $\mathrm{Ro} = 2.5$.

In all cases, the flow at the boundaries is constant from the beginning and throughout the whole simulation.

The PYREX simulations are run on the same grid as the flow past the idealized mountain. The analysis is based on the PERDOT system, taking into account all the extra radiosoundings from PYREX. An envelope orography is used and the surface roughness on the mountains is proportional to the standard deviation of the topography inside each gridbox. The PYREX simulations have been thorougly validated with the PYREX data (Beau, 1992)

The non-dimensional time unit t^* is defined as Ut/L_x, where U is the speed of the non-perturbed wind and t is the simulation time in seconds.

A more detailed description of the model and its validation for idealised orographic flows is given in ÓB96 and ÓB97.

3. The simulated drag force

The pressure drag force exerted by the airflow on the mountain in the x-direction can be expressed as:

$$\mathscr{D} = \int_{-\infty}^{+\infty} \int_{-\infty}^{+\infty} p' \frac{\partial h(x, y)}{\partial x} \, \mathrm{d}x \, \mathrm{d}y, \tag{2}$$

where p' is the pressure anomaly and $h(x, y)$ is the mountain height. The mountain exerts an equal force in the opposite direction on the atmosphere. As in most of the preceeding literature on orographic drag, we shall consider the drag positive when the flow is from left to right. Strictly speaking this is the drag force exerted on the mountain. In our exploration of the drag asymmetry we shall refer to the direction of the couple exerted by the mountain on the atmosphere. In the remaining pages of this chapter, we shall investigate the drag force calculated in our numerical experiments of flow past the elliptic mountain.

3.1. *The general flow field*

General features of the morphology of the flows with $\mathrm{Ro} \to \infty$ and $\mathrm{Ro} = 2.5$ have been described by ÓB96 and ÓB97. At low values of Nh/U, there is no stagnation on the windward slope of the mountain and there are active waves and wave breaking all along the lee slope of the mountain ridge. As Nh/U increases, the flow is blocked, strong corner winds form on each side of the mountain ridge and wave breaking ceases over the central part of the mountain, but continues on the mountain flanks. The Coriolis force breaks the symmetry and diverts

Table 1. *An overview of the simulation of flow past the bell shaped mountain*

Experiment	Nh/U	Ro	U (ms^{-1})	N (s^{-1})	h (m)	f (s^{-1})	L (m)	R
EX05	0.500	∞	10.0	0.01	500	0	4×10^4	5
EX10	1.000	∞	10.0	0.01	1000	0	4×10^4	5
EX14	1.400	∞	10.0	0.01	1400	0	4×10^4	5
EX22	2.273	∞	10.0	0.01	2273	0	4×10^4	5
EX27	2.700	∞	10.0	0.01	2700	0	4×10^4	5
EX45	4.545	∞	10.0	0.01	4545	0	4×10^4	5
EX05R25	0.500	2.5	10.0	0.01	500	10^{-4}	4×10^4	5
EX10R25	1.000	2.5	10.0	0.01	1000	10^{-4}	4×10^4	5
EX14R25	1.400	2.5	10.0	0.01	1400	10^{-4}	4×10^4	5
EX22R25	2.273	2.5	10.0	0.01	2273	10^{-4}	4×10^4	5
EX27R25	2.700	2.5	10.0	0.01	2700	10^{-4}	4×10^4	5
EX45R25	4.545	2.5	10.0	0.01	4545	10^{-4}	4×10^4	5
EX10R05	1.000	0.5	2.8	0.007	400	1.4×10^{-4}	4×10^4	5
EX27R05	2.700	0.5	2.0	0.01	540	10^{-4}	4×10^4	5
EX45R05	4.545	0.5	2.0	0.01	909	10^{-4}	4×10^4	5

The name of each experiment (first column) includes the value of the non-dimensional mountain height (Nh/U) and the Rossby number.

a greater part of the upstream flow to the left as explained by Pierrehumbert and Wyman (1985). Decreasing the Rossby number down to 0.5 does not impose qualitative changes to the flow, except that the critical value of Nh/U for the onset of upstream blocking is moved from being between 1.4 and 2.3 for $\mathrm{Ro} = 2.5$ to above 2.7 The asymmetry observed at moderate Rossby number is enhanced at $\mathrm{Ro} = 0.5$. The maximum corner wind to the left of the mountain (Fig. 1) is now $4.1U$, whereas for $\mathrm{Ro} = 2.5$ the corresponding value is only $3.5U$. There is a wide wake with weak winds, extending far downstream of the mountain. The wake is instable as can be seen in the evolution of the streamline pattern in Fig. 2. Vortices that are reminiscent of the flow in Sun and Chern (1994) and Peng et al. (1995) are created and advected downstream. Upstream of the mountain, streamlines (Fig. 2) and isobars (Fig. 3) are deflected to the left, showing resemblence to quasi-geostrophic flow (Queney, 1948; Smith, 1982), while in the lee there is a large and relatively uniform area of low pressure, extending far downstream.

3.2. Temporal variations

The temporal evolution of the total drag in the central section of the mountain is given in Fig. 4.

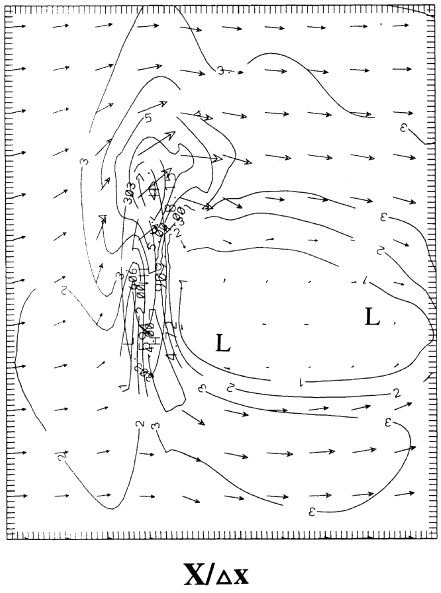

Fig. 1. The surface wind field (ms^{-1}) in EX45R05 at $t^* = 32$.

Several interesting features are revealed in this figure. For simulations with $Nh/U = 1.0$ and 4.5, decreasing Rossby number gives slightly increased fluctuations in the drag. Decreasing the Rossby number for $Nh/U = 2.7$ (going from EX27R25 to EX27R05) introduces on the other hand rapid and amplified fluctuations in the normalized value of the drag. As previously stated, EX27R25 is a blocked situation. There are stagnation points on the upstream slope, together with reversed and laterally deflected flow. Furthermore, vertically oriented vortices are formed in the lee in EX27R25. EX27R05 has no such features, and the flow is non-blocked. Bearing this in mind, Fig. 4 shows that temporal fluctuations in the drag are much more pronounced in the non-blocked regime than in the blocked flow regime. Consequently, the oscillations may be expected to be related to varying intensity of the vertically propagating gravity waves. This will be discussed later in this paper.

3.3. The mean drag

Although significant in simulations such as EX27R05, the temporal oscillations are sufficiently small to allow for meaningful comparison of a mean drag for different values of Nh/U and Ro. In the following, we compare mean drag values found by averaging the drag over one period, (such as can be seen in Fig.4), close to 15 non-dimensional time units.

Fig. 5 shows the mean drag in the central section of the flow as a function of the non-dimensional mountain height for flow with Rossby numbers 0.5, 2.5 and ∞. To the left, the flow on the nonrotating plane enters into the high drag regime as described by Miranda and James (1992) and Stein (1992). As Nh/U increases, the waves are damped and the flow enters into the blocked regime. For $Nh/U = 4.5$, the drag on the non-rotating plane has only about half its linear value. As described by ÓB97, the Coriolis force decreases the drag in the high drag state, but increases it when the flow is blocked, as it is on the right hand side of Fig. 5. At $Nh/U = 1.4$, the introduction of the Coriolis force ($\mathrm{Ro} = 2.5$) enables the flow to break out of the blocked regime by lifting the low level flow over the mountain. This is associated with the asymetric peak in the $\mathrm{Ro} = 2.5$ curve, giving drag that is greater than the drag for Ro =

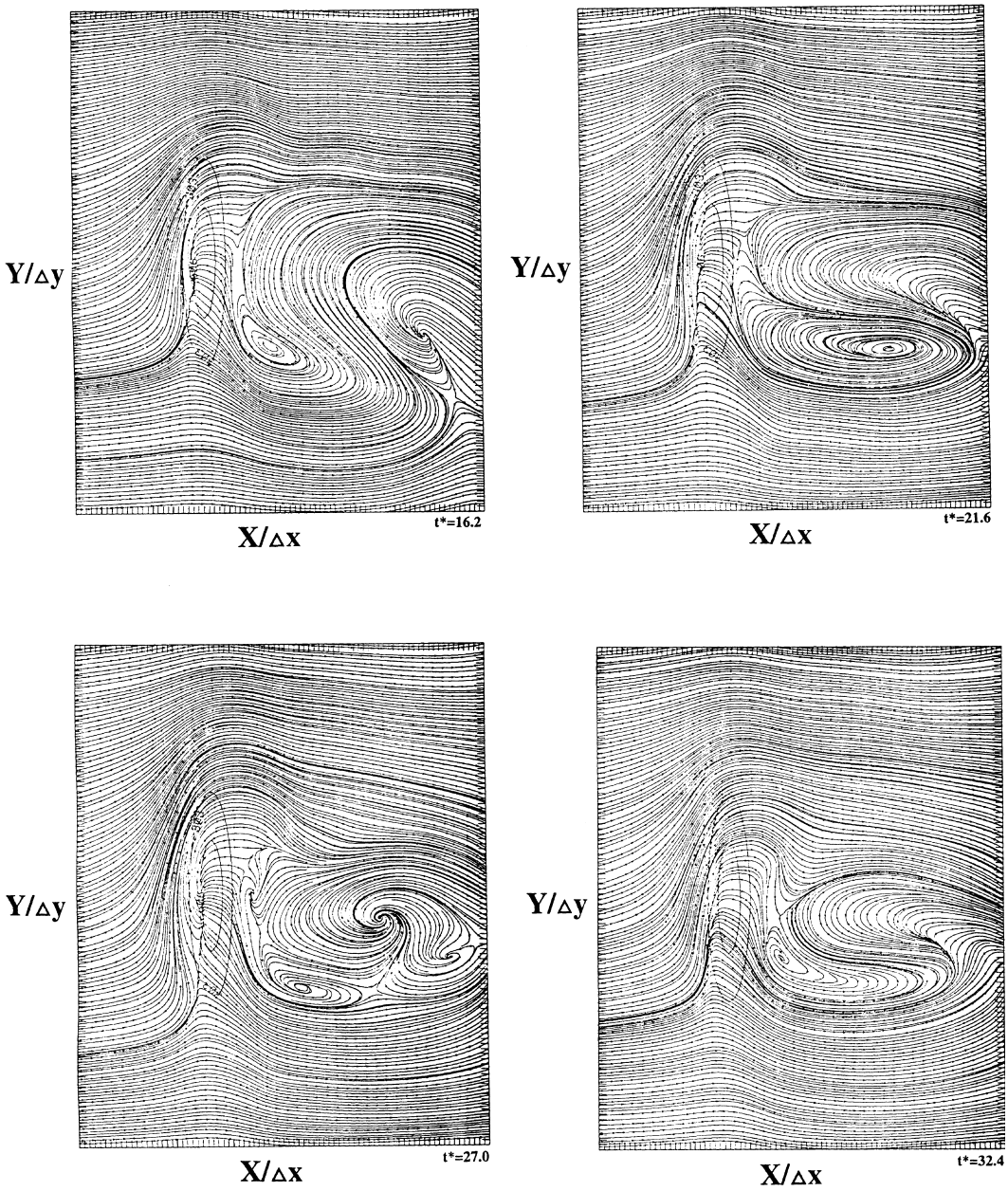

Fig. 2. Surface streamlines, showing the temporal evolution of the flow in EX45R05.

∞ at $Nh/U = 1.4$. For $\mathrm{Ro} = 0.5$, the drag of the previous high drag flow at $Nh/U = 1.0$ has been reduced to below its linear value, while a "new" high drag state is obtained by the transfer of the flow with $Nh/U = 2.7$ into a non-blocked state (EX27R05). For the blocked state ($Nh/U = 4.5$) a decrease in the Rossby number gives a regular increase in the drag and in EX45R05, the drag has passed its linear value, which is more than twofold the drag on the non-rotating plane.

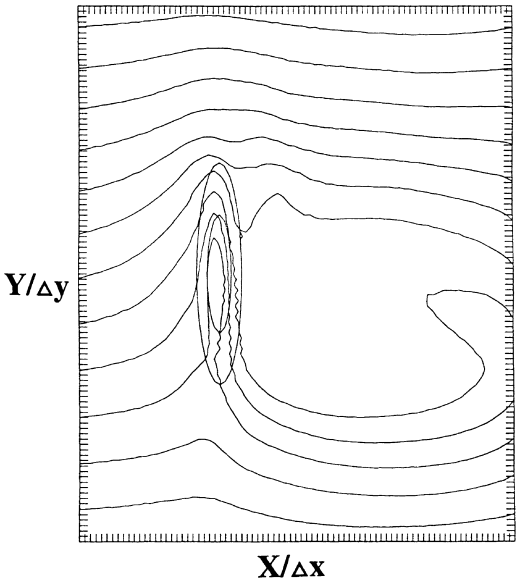

Fig. 3. The pressure field in EX45R05 at $t^* = 32$.

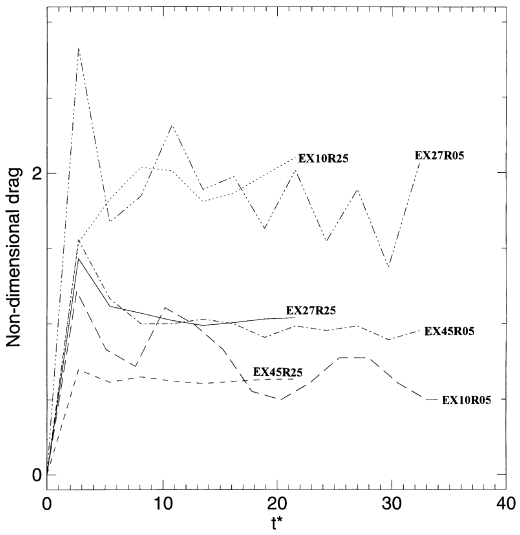

Fig. 4. Temporal evolution of the non-dimensional drag in the central section of the flow in six of the simulations presented in Table 1. The drag is normalized with its linear value $\pi\rho_0 NUh^2/4$. The non-dimensional time unit is $t^* = Ut/L_x$.

3.4. *Transversal drag (lift)*

For symetric flow on a nonrotating plane, there is no net drag force acting in the direction perpendicular to the incident flow. By introducing the Coriolis force, balanced by a large scale pressure gradient, we introduce such a perpendicular force on the mountain. This force is directed to the left and it is independent of asymmetry of the pressure anomalies created in the flow as it meets the mountain. We shall call this a lift force due to the background flow (Smith, 1979a). By breaking the symmetry of the flow, we influence the lift force in our experiments. Schär and Durran (1997) studied the transversal component of the drag in experiments where asymmetry was introduced by anomalies in the upstream temperature field (at $f = 0$). For blocked flow, they found the transversal drag to oscillate between positive and negative values at the same frequency as the vortex shedding which they also observed. In our simulations with the Coriolis force, the transversal drag remains relatively stable, but as shown in Fig. 6, it clearly depends on both Nh/U and Ro, and is sensitive to the flow regime as it decreases

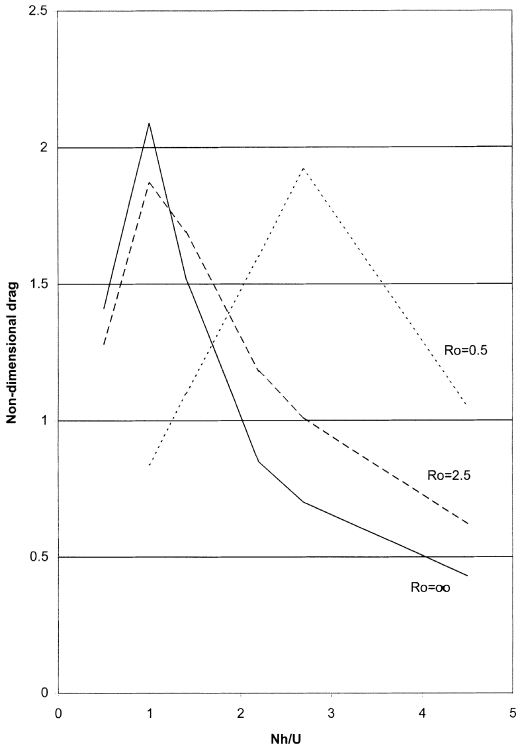

Fig. 5. Non-dimensional drag as a function of Nh/U for three series of simulations with different value of the Rossby number. The drag is normalized with its linear value $\pi\rho_0 NUh^2/4$.

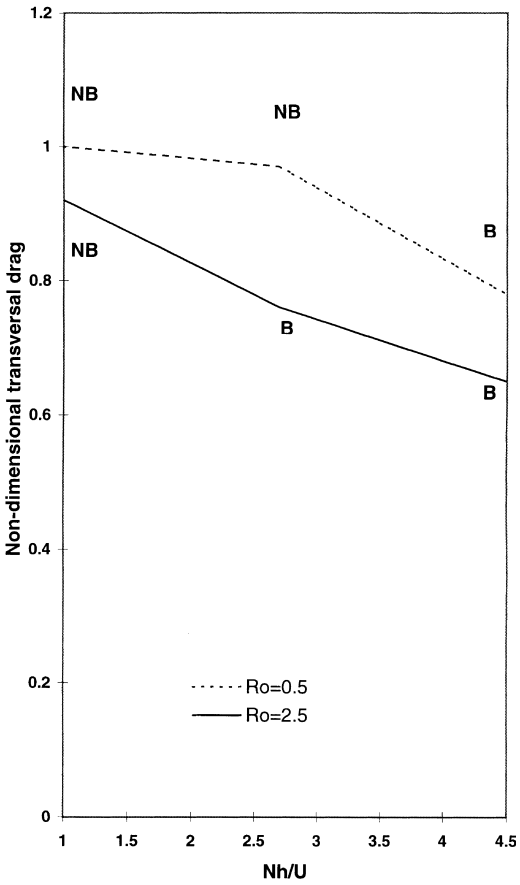

Fig. 6. Transversal drag as a function of Nh/U for Ro = 2.5 and Ro = 0.5. The drag is normalized with the drag due to the background pressure gradient (Smith, 1982). **B** indicates a simulation with blocked flow and **NB** a simulation with nonblocked flow.

more rapidly for increasing Nh/U when the flow is entering the blocked regime. An increase in the Rossby number results in lower normalized lift force for all values of Nh/U. The large impact the flow perturbation has on the lift force in EX45R05 is easily understood from the wind and pressure field in Fig. 1. and Fig. 3. The upstream low level flow is to a great extent diverted to the left, giving a surplus of dense air and high pressure relative to the right flank.

3.5. *Asymmetry of the drag*

The temporal evolution of the couple is given in Fig. 7. The figure shows the proportion of the

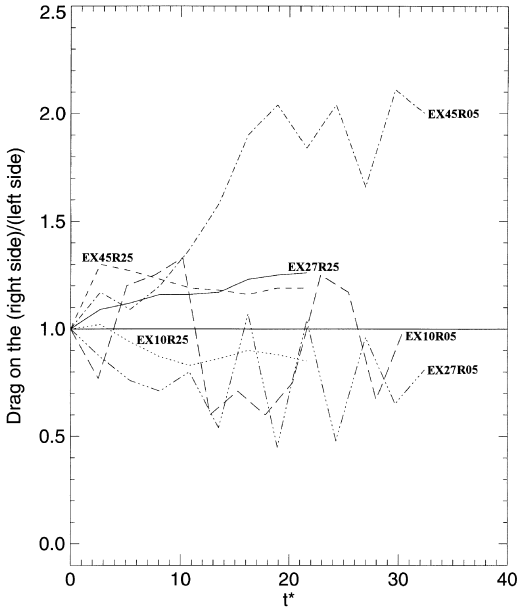

Fig. 7. Temporal evolution of the proportion of the drag on the right side of the bell shaped mountain to the drag on the left side of the same mountain in six of the simulations presented in Table 1. The non-dimensional time unit is $t^* = Ut/L$.

drag on the right hand side to the drag on the left side of the central section of the flow (facing downstream). The sections to the right and left are taken at a distance of half a half-width from the central section. Fig. 7 reveals a similiar dependence on the Rossby number and flow regime as does the drag in the central section displayed in Fig. 4. The greatest oscillations are found in the non-blocked flows. This is particularly clear for $Nh/U = 2.7$. When the Rossby number is reduced from 2.5 down to 0.5 and the flow is no longer blocked significant oscillations occur. From the other simulations, high Rossby number appears to damp the temporal oscillations, but this is however less clear and longer integration would be needed to draw firm conclusions on this.

In the non-blocked flows, the main contribution to the drag is through the vertically propagating waves and a close inspection of the isentropes (not shown) reveals that the oscillations are mainly due to variations in wave activity, and not in the density of the low level flow. The curves in Fig. 7 also show that the drag in the non-blocked flows tends to be greater on the left flank of the moun-

tain, while the right part of the mountain gives greater drag for the blocked flows. In other words, *the mountain exerts a cyclonic couple on the atmosphere in non-blocked flows and an anticyclonic couple in blocked flows.* The lower the Rossby number is, the greater is the change in the couple as the flow changes regime and in the simulation with the highest value of Nh/U and the lowest value of the Rossby number (EX45R05), the drag on the right hand side is about twice the drag on the left side in the same experiment. This may be the most interesting result of this paper and will be discussed further in the following section.

4. Why do the temporal fluctuations and the couple depend on the flow regime?

4.1. Temporal fluctuations

In all our simulations with non-blocked flow, there are strong breaking waves over the central part of the mountain. The wave breaking process is in itself a process of oscillations between wave breaking and buildup and therefore the temporal fluctuations in the drag of the non-blocked flows are not surprising. However, oscillations of flow speed in the upstream blocking are also well known (Pierrehumbert and Wyman, 1985; ÓB96). Such oscillations do not necessarily have a great impact on the drag and our simulations indicate that they are small compared to the fluctuations in wave activity. Upstream fluctuations in wind speed may in fact also influence the secondary wave breaking on the flanks of the mountain. The simulations featuring blocked flow do all have secondary wave breaking, in particular on the left flank of the mountain. This explains the fluctuations in the strength of the couple in EX45R05 (Fig. 7), a characteristic that is not reflected in the drag on the central part of the mountain (Fig. 4). Unlike in Schär and Durran (1997), the vortex shedding in the wake appears not to lead to strong oscillations in the drag. This may be explained by the fact that where the Coriolis force is present, a greater part of the drag in blocked flows comes from the upstream pressure anomaly and that the instability in the lee is inside a fairly well defined wake with very low speeds (Figs. 1, 2). Due to the low flow speeds, fluctuations in wind direction do not necessarily result in large movements of mass.

4.2. The asymmetry in non-blocked and blocked flows

The tendency for greater drag on the left side in the non-blocked flows may be explained by refering to the Coriolis force diverting a relatively great part of the flow to the left, giving greater flow speed and wave activity over the left flank, than over the right flank of the mountain, but how can we explain the physics behind the anticyclonic couple in the blocked flows?

Numerical simulations of quasi-geostrophic non-linear flow past an isolated mountain by Verron and Le Provost (1985) gave an asymetric flow field and vorticity pattern that correspond to the anticyclonic couple presented here (their Figs. 4, 5). The Verron and Le Provost simulations were performed of rigid-lid flow with flow parameters that correspond to lower Rossby numbers and higher non-dimensional mountain height than in our experiments, confirming that the anticyclonic couple is indeed not a result of gravity wave pressure anomalies.

ÓB97 studied the pressure anomalies in a blocked case with moderate Rossby number and found the main contribution to the anticyclonic couple to come from dense air on the left lee side of the mountain. In their Fig. 12 there is a permanent downward deflection of the pressure curves in the lee to the right, which corresponds to a downward deflection of the isentropes on the right side of the mountain in their Fig. 2. The asymmetry of the upstream pressure field gives rise on the other hand rise to a cyclonic couple. The reason for the asymmetry remained however rather obscure as well as its connection with the Rossby number and the flow regime. In view of the results of ÓB97, we shall focus on the low level density anomalies. Fig. 8 confirms the surplus of dense air above the left lee slope and that the accumulation of this low level dense air is associated with strong upward motion. Our simulations indicate stronger anticyclonic couple for lower Rossby number, as long as the flow remains blocked. This suggests that the stronger the geostrophic adjustment is, the greater is the strength of the couple. Yet, there is no drag and consequently no couple predicted by geostrophic theory (Queney, 1948). This is explained by the failure of the theory to account for the upstream blocking.

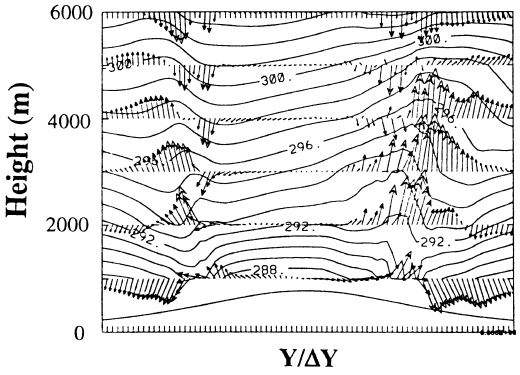

Fig. 8. Isentropes (K) and wind arrows in the plane of a cross section transverse to the incident flow, one and a half half-width downstream of the mountain in EX45R25. The reader faces the incident flow (left becomes right).

The upward motion in Fig. 8 is related to horizontal convergence above the lee slope which is clearly greater on left than than on the right hand side (Fig. 1). This horizontal convergence can be explained by geostrophic adjustment of the flow to the pressure field in Fig. 3.

The upstream flow that is deflected to the left is accelerated where the horizontal pressure gradient increases. At the crest of the left mountain flank, the pressure gradient is greatest and a very short distance downstream there is a maximum in the wind field. Over the left lee slope, the pressure gradient decreases rapidly and the flow decelerates. Over the right flank of the mountain, we find the opposite situation, there is a relatively weak pressure gradient on the upstream side, while once the flow has passed the crest it enters a region of strong pressure gradient and accelerates.

5. Asymmetry of the drag in real flows

5.1. Introduction

In the preceeding sections, the experiments have been set up to give clear and significant drag asymmetry, by using an elongated mountain perpendicular to the incoming flow. Although the couple is relevant for such flows, its importance in the real atmosphere is so far unknown. For high mountains that generate a blocking most of the time, we expect a more or less permanent anticyclonic couple, while for lower mountains in windy regions with frequent change between flow regimes the direction of the couple should vary accordingly. In the following we shall investigate data from a field campaign in the Pyrenees and observations from the regular observation network in Iceland. These observations will be discussed and interpreted in view of our results on the couple.

5.2. PYREX

In the fall of 1990, an extensive field experiment named PYREX took place around the Pyrenean mountain range. The main purpose of PYREX was to measure the deceleration of the atmosphere due to orographically generated flow perturbations. The PYREX observations consisted of frequent radiosoundings from a dense network of sounding sites, microbarographs situated on an axis crossing the central part of the mountain range, as well as measurements made by research aircrafts. So far, the PYREX database has served for a wide range of research of orographic flows (Bougeault et al., 1997) and it will undoubtedly be of help in many future projects.

To test our results on the couple in more realistic flows, we have simulated two IOPs from PYREX, one with northerly flow (IOP9) and one with southerly flow (IOP3). In both cases, the low level flow is blocked and deflected around the mountain range. The total drag in the direction of the flow is calculated in the two boxes shown in Fig. 9. As before, left and right are defined by looking in the direction of the flow. In other words, the left box is the westerly (Atlantic) one for southerly flow, while for northerly flow, the left box is the one to the east (Mediterranean). The Pyrenees are, as other mountains on the Earth, asymetric. In the east, the mountain range ends in rather steep slopes at the Mediterranean Sea, while in the west, the slopes are not as steep and the mountain range is continued by the Cantabric chain. Consequently, low level flow from the north is more easily blocked by the western part of the Pyrenean mountains, and the drag in this part is favoured when compared to the eastern part.

Fig. 11 shows the proportion of drag in the right box to the drag in the left box as a function of the Rossby number for both the IOPs. The

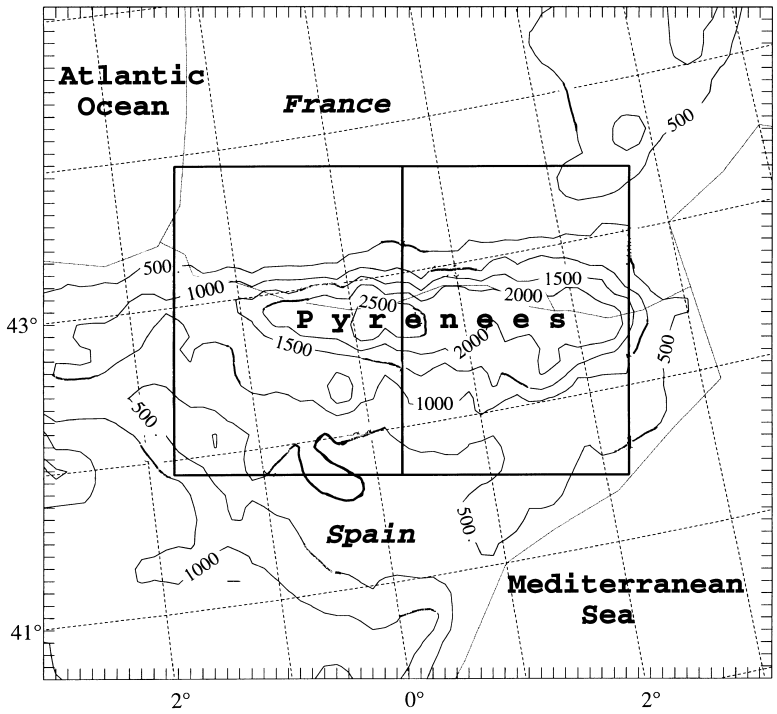

Fig. 9. A topographic map of the Pyrenees showing the boxes where the drag on the left and the right side of the mountain range is calculated.

Rossby number is calculated by averaging the wind component perpendicular to the mountain range between the surface and $z = h$ in a place 180 km upstream of the central part of the mountains. The time of advection from this point to the mountain top is of the order of 3 hours and in Fig. 10, we compare the Rossby number of the flow to the drag calculated 3 hours later.

In the case of the northerly flow, there is a clear linear correlation between the Rossby number and the couple in Fig. 10. As in the idealized flows, the couple increases for decreasing Rossby number and for Rossby numbers increasing from a little less than 1 to 2, the proportion of the drag in the right box to the drag in the left box decreases from more than 2.5 to less than 1.5. In the case of southerly flow, the drag is not favoured in the west. We expect this to be related to much less dense low level air than in the northerly flow. Yet, a decrease in the Rossby number is associated with a greater proportion of the drag from the right part of the mountain, just as is the case in the northerly flow and in the idealized flows.

5.3. Iceland

The asymmetry of the drag has also been investigated in northerly flow impinging on Iceland. Here, the drag evaluation is based on surface pressure observations at 4 coastal stations and observations from Grímsey island are considered to be representative for the upstream wind. The location of the stations is shown together with the topography of Iceland in Fig. 11. We consider a sample of all days during the year 1996 when the wind direction at noon in Grímsey is between NNW and NNE, including both directions. Fig. 12 compares the wind speed in Grímsey to pressure observations 3 hours later. The pressure drag on the right-hand side (facing downstream as before) is considered to be P (Gjögur)–P (Reykjanesviti) and the pressure drag to the left is P(Raufarhöfn)–P(Akurnes). Five cases with Drag(right side/left side) falling outside the range 0–4 have been neglected, since they represent weather situations where the northerly wind in Grímsey is far from representing the synoptic weather situation over

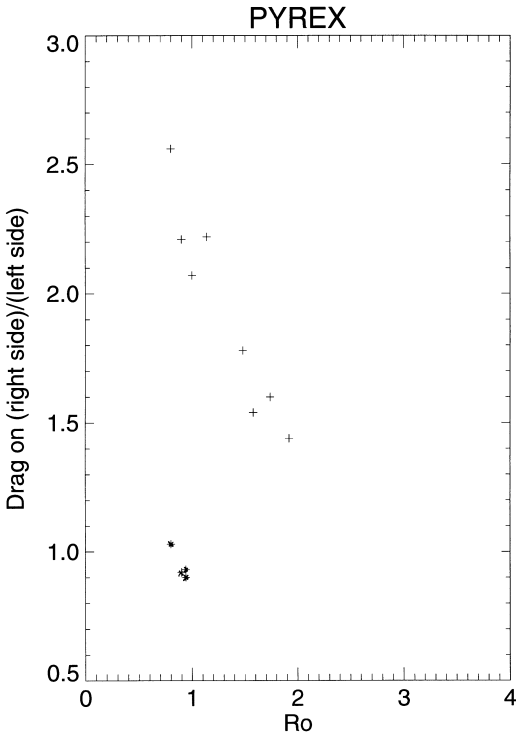

Fig. 10. Drag in the right hand box divided with the drag in the left box in Fig. 8 during IOP3 (stars) and IOP9 (crosses) in PYREX. IOP3 featured southerly flow on 15 October 1990 and IOP9 was an episode of northerly flow from 15 November 1990 to 16 November 1990. The drag is calculated at 03, 06, 09 and 12 UTC and is plotted against the Rossby number.

the whole of Iceland. The remaining cases are plotted in Fig. 12 as a function of the Rossby number, which is calculated by dividing the observed surface wind in Grimsey with 0.8 and considering the length scale or mountain half-width to be 100 km.

The figure reveals a clear tendency for greater drag on the right side for low values of the Rossby numbers, while high Rossby numbers give greater drag on the left side. If we consider separately the cases with $\mathrm{Ro} < 0.85$ and $\mathrm{Ro} > 0.85$, we find 10 cases out of 12 to give greater drag on the right hand side for the first group, while for the higher Rossby numbers, 8 out of 10 cases give greater drag on the left side. The mean proportion right/left is 1.41 for the lower Rossby numbers, while for the cases with $\mathrm{Ro} > 0.85$, the mean drag on the right side is 0.60 times the mean drag on the left side. The populations of the two groups are indeed different with a high degree of confidence. There is, however, not a clear correlation between the couple and the Rossby number within each of the two groups. Rossby number 0.85 corresponds to $U = 11.3\ \mathrm{ms}^{-1}$ and Nh/U close to 2.5, provided that N is constant. However strange assumption that may be for real-world flows, investigation of atmospheric stability in northerly flow over Keflavik (close to Reykjanesviti) shows the general variation to be no more then $\pm 10\%$, which is an order of magnitude smaller than the variations in wind speed. This is different from southerly winds in Iceland that vary from very stable air from the south or the southeast to extremely unstable airmasses in wintertime soutwesterly flow. The small variations in stability of the north wind is explained by the fact that advection of very warm air is hardly ever associated with northerly winds and in the wintertime, the distance to the ice edge is not far enough for the coldest airmasses to develop a deep convective layer. The Nh/U value of 2.5 corresponds quite well with the regime transition from blocked to non-blocked flow found to be at $2.7 < Nh/U < 4.5$ for $\mathrm{Ro} = 0.5$ (Section 3) and at $1.4 < Nh/U < 2.3$ for $\mathrm{Ro} = 2.5$ (ÓB97).

6. Summary and discussion

The simulations of flow past the elliptic mountain have shown significant variations of the contribution of the left and right part of the mountain to the orographic drag force and that the relative contribution of the flanks depends on the flow regime. In non-blocked flows, the mountain exerts a cyclonic couple on the flow, while in blocked flows, the couple is anticyclonic. The couple is strengthened by low Rossby number. The cyclonic couple in non-blocked flows is related to enhanced wave activity on the left flank of the mountain, while the anticyclonic couple is mostly due to dense air over the left lee slope. The paper proposes a simple explanation of this, based on the geostrophic adjustment of the flow to the mountain induced pressure field, giving horizontal convergence with upward motion and accumulation of low level dense air above the left lee slope. The anticyclonic couple corresponds to the vorticity

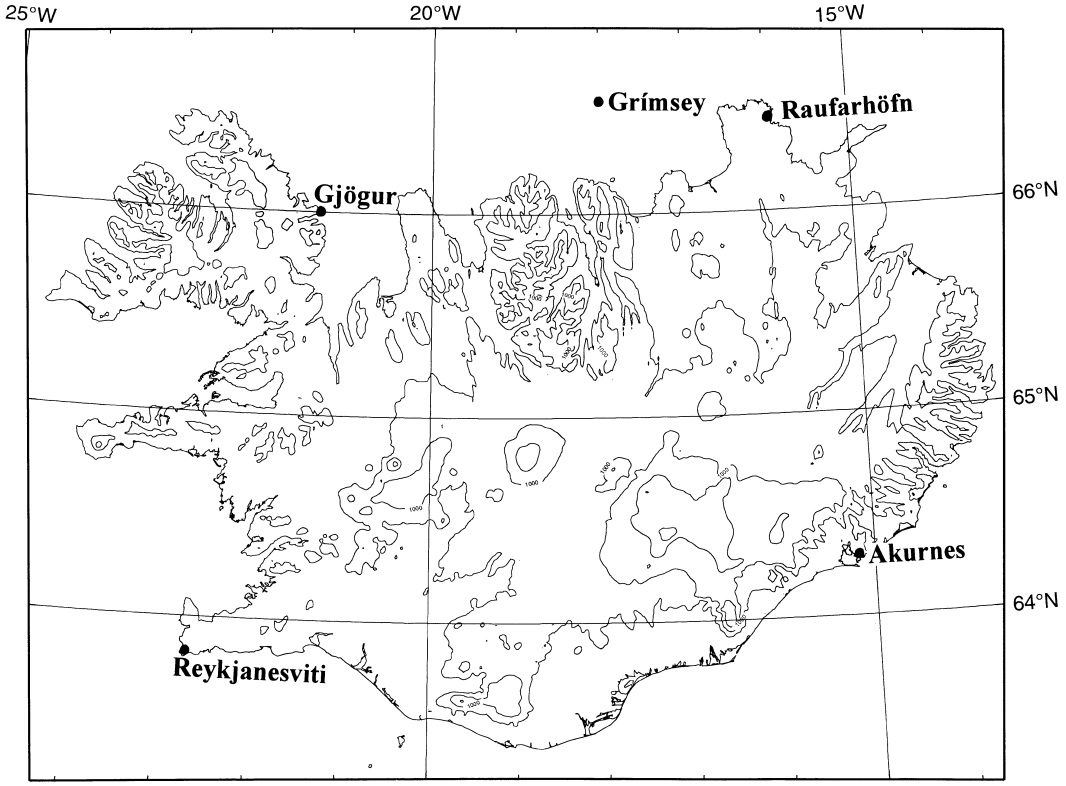

Fig. 11. A topographic map of Iceland (500-m contours) showing the location of the observing stations.

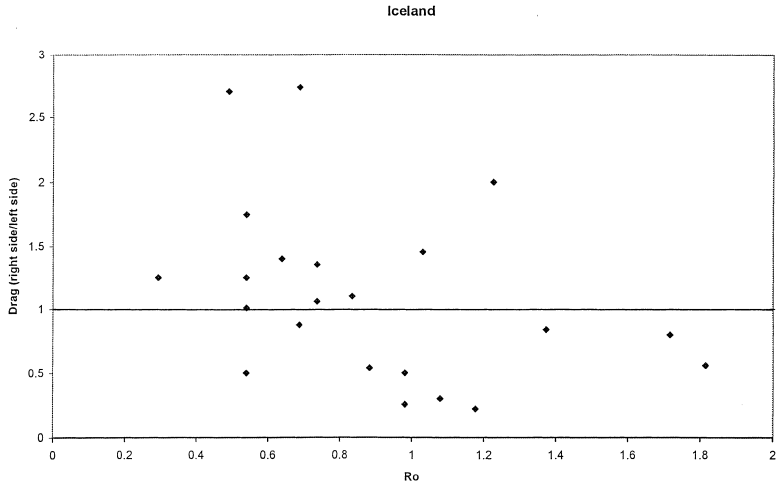

Fig. 12. Drag on the right hand side divided with the drag on the left side of Iceland and plotted against the Rossby number. The drag on the right hand side is represented by the pressure at Raufarhöfn — pressure at Akurnes and the drag on the left side is pressure at Gjögur — pressure at Reykjanesviti.

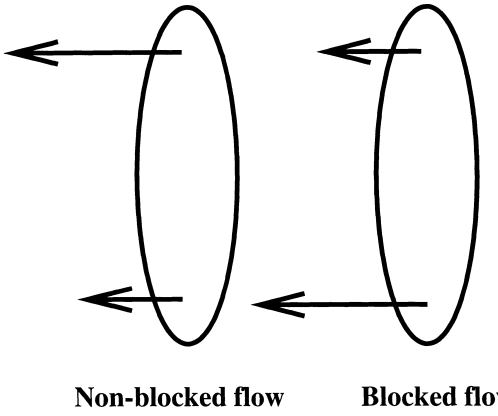

Fig. 13. A schematic overview of the couple at the presence of the Coriolis force.

field simulated by Verron and Le Provost (1985). The couples are shown schematically in Fig. 13.

We observe, in the idealized experiments, significant temporal oscillations of the drag in non-blocked flows. Blocking of the low level flows has a strong damping effect on these oscillations, indicating that the oscillations are mainly related to variations in the wave activity (wave breaking) over the obstacle.

Laboratory experiments by Boyer et al. (1987) showed stronger wave activity on the right side of an obstacle in rotating flows, which is opposite to what we simulate. The experiments by Boyer et al. (1987) had Rossby number as low as 0.3 which is lower than in all our simulations, indicating that in non-blocked flows at very low Rossby numbers, the couple may by anticyclonic instead of cyclonic.

Previous results (Thorsteinsson and Sigurdsson, 1996; ÓB97) on the delaying impact of the Coriolis force on the onset of upstream blocking are confirmed and at $\mathrm{Ro} = 0.5$, flow with Nh/U as high as 2.7 is not blocked. A new high-drag state is created, whereas the waves in the old high drag state $Nh/U \sim 1$ are reduced by the rotation.

At $\mathrm{Ro} = 0.5$, the lift force of the background flow is reduced significantly as the flow enters the blocked regime. This impact of regime transition is less clear at $\mathrm{Ro} = 2.5$, where the lift force is reduced more gradually for increasing Nh/U.

Two independent studies of simulated real flow from PYREX and of observations around Iceland suggest that the results from the idealised experiments concerning the couple are highly relevant to explain the behaviour of the real atmosphere, flowing over complex orography. The PYREX flow is blocked and the couple becomes more anticyclonic for decreasing Rossby number. The flow around Iceland shows on the other hand a clear sign of regime transition; for low values of Nh/U, the couple is in most cases cyclonic, while for the higher values of Nh/U it is predominantly anticyclonic. This result gives an important insight into the varying shape of the Icelandic lee-trough, which has been a puzzle for forecasters for decades.

The impact of non-resolved orography is commonly parameterised in numerical models of the atmosphere. Evolution in this field is directed towards studies of the blocking phenomenon and different effects of blocked and non-blocked flow. Lott and Miller (1997) have constructed a new parameterisation for the ECMWF model, with explicit treatment of the blocked flow. Their scheme was validated with real blocked flow from PYREX. Beau and Bougeault (1998) have also studied the behaviour of a drag parameterisation with respect to increased blocking effect in real flows. The present results from the idealized, as well as real flows suggest that further improvements of the parameterisation schemes could be done by including the couple and its dependence on flow regime and Rossby number. This may lead to a more correct representation of vorticity in the lee of mountains which can be of vital importance for short range weather forecasts (Ólafsson, 1998). The impact of blocking and low Rossby number for the lift force is also of interest in this context, not only for mesoscale flows, but also on a larger scale. Forcing of Rossby waves is related to the lift force and our simulations show that nonlinearities reduce the lift force exerted on the mountain, suggesting that linear models of topographic Rossby waves may give erroneus estimation such waves or of their importance in the large scale flow.

7. Acknowledgements

The author ackowledges both helpful discussions on the nature of blocked flows with Julian C. R. Hunt and comments and suggestions from anonymous reviewers. He also wishes to thank CNRM, Météo-France, for providing computing facilities and access to the PYREX database. The

PYREX experiment was made possible by the participation of a large number of institutes from France, Spain and Germany. It was funded by Météo-France, the Instituto National de Meteorologia (Spain), the Institut National des Sciences de l'Univers (ARAT, PAMOS and PAMOY programs), the Centre National d'Etudes Spatiales, Electricité de France, Region Midi-Pyrenees and the Deutsche Forschungsanstalt fuer Luft und Raumfahrt. The Icelandic observations come from the regular observation network of the Icelandic Meteorological Office (Vedurstofa Íslands). A part of this study was undertaken with the help of the Icelandic Research Council (RANNÍS).

REFERENCES

Beau, I, 1992. *Evaluation des paramétrisations de l'effet orographique sous maille dans les modeles de circulation génŕale a l'aide de PERIDOT 10 km.* Tech. Rep. Ecole Nationale de la Météorologie, Toulouse. Available from CNRM, 31057, Toulouse, France.

Beau, I. and Bougeault, P. 1998. Asessment of a gravity-wave drag parameterisation with the PYREX data. *Quart. J. Roy. Meteor. Soc.* **124**, 1443–1464.

Bessemoulin, P., Bougeault, P., Genoves, A., Clar, A. J. and Puech, D. 1993. Mountain pressure drag during PYREX. *Beitr. Phys. Atmos.* **66**, 305–325.

Bougeault, P. and Lacarrere, P. 1989. Parameterization of orography induced turbulence in a meso-beta-scale model. *Mon. Wea. Rev.* **117**, 1872–1890.

Bougeault, P., Benech, B., Bessemoulin, P., Carissimo, B., Clar, A. J., Pelon, J., Petitdidier, M. and Richard, E. 1997. PYREX: a summary of findings. *Bull. Amer. Meteor. Soc.* **79**.

Bougeault, P., Bret, B., Lacarrere, P. and Noilhan, J. 1991. An experiment with an advanced surface parameterisation in a mesobeta-scale model: Part II: The 16 June simulation. *Mon. Wea. Rev.* **119**, 2374–2392.

Bougeault, P., Jansa, A., Attié, J., Beau, I., Bénech, B., Benoit, R., Bessemoulin, P., Caccia, J. L., Campins, J., Carissimo, B., Champeaux, J. L., Crochet, M., Druilhet, A., Durand, P., Ekhalfi, A., Flamant, P., Genoves, A., Georgelin, M., Hoinka, K. P., Klaus, V., Koffi, E., Kotron, V., Mazaudier, C., Pelon, J., Petitdidier, M., Pointin, Y., Puech, D., Richard, E., Satomura, T., Stein, J. and Tannhauser, D. 1993. The atmospheric momentum budget over a major mountain range: first results of the PYREX field program. *Annales Geophysicae* **11**, 395–418.

Boyer, D. L., Davies, P. A., Holland, W. R., Biolley, F. and Honji, H. 1987. Stratified flow over and around isolated three-dimensional topography. *Philos. Transactions of the Royal. Soc. of London* **322**, 213–241, no. 1564.

Broad, A. 1996. High-resolution numerical model integration to validate gravity wave drag parametrisation schemes: a case study. *Quart. J. Roy. Meteor. Soc.* **122**, 1625–1653.

Durran, D. R. 1990. Mountain waves and downslope winds. In: *Meteorological monographs: atmospheric processes over complex terrain*, ed. W. Blumen. Amer. Meteor. Soc., pp. 59–81.

Eliassen, A. and Palm, E. 1960. On the transfert of energy in stationary mountain waves. *Geophys. Norv.* **22**, 1–23.

Gill, A. E. 1982. *Atmosphere ocean dynamics.* Academic Press, New York, 662 pp.

Imbard, M., Joly, A. and du Vachat, R. 1986. *Le modele de prévision numérique PERIDOT: formulation dynamique et modes de fonctionnement*. Technical Report 161 EERM (available from CNRM, F 31057, Toulouse, France).

Klemp, J. B. and Lilly, D. K. 1978. Numerical simuation of hydrostatic mountain waves. *J. Atmos. Sci.* **32**, 320–339.

Lott, F. and Miller, M. J. 1997. A new subgrid scale orographic drag parametrisation: its formulation and testing. *Quart. J. Roy. Meteor. Soc.* **123**, 101–128.

Miranda, P. M. A. and James, I. N. 1992. Non-linear three-dimensional effects on gravity-wave drag: splitting flow and breaking waves. *Quart. J. Roy. Meteor. Soc.* **118**, 1057–1081.

Ólafsson, H. 1998. Different predictions by two NWP models of the surface pressure field east of Iceland. *Meteorol. Apps.* **5**, 253–261.

Ólafsson, H. and Bougeault, P. 1996. Nonlinear flow past an elliptic mountain ridge. *J. Atmos. Sci.* **53**, 2465–2489.

Ólafsson, H. and Bougeault, P. 1997. The effect of rotation and surface friction on orographic drag. *J. Atmos. Sci.* **54**, 193–210.

Peng, M. S., Li, S.-W., Chang, S. W. and Williams, R. T. 1995. Flow over mountains: Coriolis force, transient troughs and three dimensionality. *Quart. J. Roy. Meteor. Soc.* **121**, 593–614.

Pierrehumbert, R. T. and Wyman, B. 1985. Upstream effects of mesoscale mountains. *J. Atmos. Sci.* **42**, 977–1003.

Queney, P. 1948. The problem of the airflow over mountains. A summary of theoretical studies. *Bull. Amer. Meteor. Soc.* **29**, 16–26.

Schär, C. and Durran, D. R. 1997. Vortex formation and vortex shedding in continously stratified flows past isolated topography. *J. Atmos. Sci.* **54**, 534–554.

Shutts, G. 1998. Idealized models of the pressure drag force on mesoscale mountain ridges. *Contrib. Atmos. Phys./Beitr. Atmos. Phys.* **71**, 303–346.

Smith, R. B. 1979a. Some aspects of the quasi-

geostrophic flow over mountains. *J. Atmos. Sci.* **36**, 2385–2393.

Smith, R. B. 1979b. The influence of the Earth's rotation on mountain wave drag. *J. Atmos. Sci.* **36**, 177–180.

Smith, R. B. 1982. Synoptic observations and theory of orogrphy disturbed wind and pressure. *J. Atmos. Sci.* **30**, 60–70.

Smith, R. B. 1989. Hydrostatic airflow over mountains. In: *Advances in geophysics*, **53**. Academic Press, pp. 59–81.

Smith. R. B. and Grønås, S. 1993. Stagnation points and bifurcation in 3-D mountain airflow. *Tellus* **45A**, 28–43.

Stein, J. 1992. Investigation of the regime diagram of hydrostatic flow over a mountain with a primitive equations model. Part I: Two dimensional flows. *Mon. Wea. Rev.* **120**, 2962–2976.

Sun, W. Y. and Chern, J. D. 1994. Numerical experiments of vortices in the wakes of large idealized mountains. *J. Atmos. Sci.* **50**, 191–209.

Thorsteinsson, S. and Sigurdsson, S. 1996. Orogenic blocking and deflection of stratified air flow on an f-plane. *Tellus* **48A**, 572–583.

Verron, J. and Le Provost, C. 1985. A numerical study of quasi-geostrophic flow over isolated topography. *J. Fluid Mech.* **154**, 231–252.